

The influence of GDL wettability on DMFC performance: A combined local current distribution and high resolution neutron radiography study

Alexander Schröder^a, Klaus Wippermann^a, Werner Lehnert^a, Detlef Stolten^a,
Tilman Sanders^b, Thorsten Baumhöfer^b,
Nikolay Kardjilov^c, André Hilger^c, John Banhart^c, Ingo Manke^c

^aInstitute of Energy Research, IEF-3: Fuel Cells, Forschungszentrum Jülich GmbH,
52425 Jülich, Germany

^bInstitute for Power Electronics and Electrical Drives (ISEA), RWTH Aachen University,
Jägerstr. 17-19, 52066 Aachen, Germany

^cHelmholtz Centre Berlin (Hahn-Meitner-Institute), SF3,
Glienicker Str. 100, 14109 Berlin, Germany

Abstract

The influence of the anode and cathode GDL wettability on the current and media distribution was studied using combined *in situ* high resolution neutron radiography and locally resolved current distribution measurements. MEAs were prepared by vertically splitting either the anode or cathode carbon cloth into a less hydrophobic part (untreated carbon cloth ‘as received’) and a more hydrophobic part (carbon cloth impregnated by PTFE dispersion). MEAs with partitioned anode carbon cloth revealed no difference between the untreated and the hydrophobised part of the cell concerning the fluid and current distribution. The power generation of both parts was almost equal and the cell performance was similar to that of an undivided MEA (110 mW/cm², 300 mA/cm², 70 °C). In contrast, MEAs with partitioned cathode carbon cloth showed a better performance for the hydrophobised part, which contributed to about 60 % of the overall power generation. This is explained by facilitated oxygen transport especially in the hydrophobised part of the cathode gas diffusion layer. At an average current density of 300 mA/cm², a pronounced flooding of the cathode flow field channels adjacent to the untreated part of GDL led to a further loss of performance in this part of the cell. The low power density of the untreated part caused a significant loss of cell performance, which amounted to less than 40 mW/cm² (at 300 mA/cm²).

* Corresponding author. Tel.: +49 2461 61-1579; fax: +49 61-6695.
E-mail address: a.schroeder@fz-juelich.de (A. Schröder).

Keywords: DMFC; High resolution neutron radiography; Current distribution; Fluid distribution; wettability; hydrophobic properties; GDL

1. Introduction

The gas diffusion layer (GDL) is the mediator between the nanostructured electrode and the flow field with structures in the mm range. Besides providing passages for methanol on the anode side and oxygen on the cathode side, the GDL is responsible for the product removal from the electrochemically active area to the flow field channels.

On the cathode side of a liquid fuelled DMFC, the flooding is more pronounced than in a PEFC, since the water is not only produced on the cathode side but permeates through the membrane additionally, driven by a concentration gradient and electroosmotic drag. On the anode side, the blocking effects of CO₂ bubbles may lead to a disturbance of the methanol supply. These two phase flow effects do not only play a crucial role inside the GDL but also in the flow field channels. Due to the interaction between GDL and flow field, different GDLs result in altered fluid distributions inside the cell and therefore in different operating behaviours [1].

Uneven fluid distributions cause inhomogeneous current distributions which may lead to a significant power loss and accelerated degradation of the fuel cell. In order to investigate the effects leading to inhomogeneous current distributions, a measurement technique is mandatory, that allows the *in situ* observation of the current, CO₂ and water distribution simultaneously.

The use of segmented printed circuit boards (PCBs) is a well-established technique for measuring local currents in fuel cells. The features and advantages of our self-developed set up, which is based on printed circuit board technology, are described in [2] (see also section 'Experimental'). It allows the accurate measurement of up to 54 segment currents and

impedances based on compensated sensor resistors [3].

Several methods have been reported in the literature to observe the CO₂ and water distribution *in situ* under operating conditions of PEFCs and DMFCs. Some authors used cells with a transparent cover to observe the carbon dioxide evolution and the two phase flow behaviour visually [4–11]. A further method is synchrotron X-ray radiography [12–15]. In order to use a completely non invasive method for the observation of CO₂ and water, we used neutron radiography which has proved its applicability for a variety of questions [16–22]. Neutron radiation has a high attenuation coefficient for hydrogen compared to the one of most metals. The neutron beam is less affected by the solid cell components compared to liquid water which leads to a strong attenuation of the beam. Thus, the distribution of hydrogen-rich species can be observed during operation. In our recent paper, the combination of *in situ* high resolution neutron radiography and segmented current distribution measurement was identified as a suitable tool to correlate current and fluid distribution in DMFCs [23].

The intention of the present work is to study the influence of the anode and cathode GDL wettability on the current and media distribution using combined *in situ* high resolution neutron radiography and current distribution measurements. To visualize the difference between untreated and hydrophobised parts of the cell, either the anode or cathode GDL is vertically split into a less and a more hydrophobic part. The procedure of vertically splitting GDLs is justified, as the current distribution on the left and the right side of cells with undivided membrane electrode assemblies (MEAs) is almost even. A horizontal splitting of the GDLs would not be useful, since the media and current distribution of the upper and lower part of the cell is considerably different, caused by an accumulation of CO₂ in the top part of the cell and flooding in the middle and bottom part of the cell.

2. Experimental

2.1 Preparation of MEAs

The functional layers of the used MEAs with an active area of $4.2 \times 4.2 \text{ cm}^2$ were prepared onto carbon cloth (Ballard). Both hydrophobised and untreated carbon cloth material with microporous layer was used as gas diffusion layer for the electrodes. To compare hydrophobised and untreated GDLs in the same cell under operating conditions, either the anode or cathode GDL was vertically split into an untreated left part and a hydrophobised right part (see scheme in Fig. 1). To avoid an interaction of anode and cathode effects, the corresponding counter electrode was always undivided and hydrophobised.

As functional layers, first a hydrophobised microporous layer and then either the anode or cathode catalyst layer were prepared on the carbon cloth substrates by knife-over-roll technique. The microporous layer consisted of 60 wt.% carbon (Cabot) and 40 wt.% PTFE. The anode catalyst consisted of 75 wt.% Pt/Ru and 25 wt.% carbon (Johnson Matthey). The Pt/Ru loading of the anodes was about 2 mg cm^{-2} . The cathode catalyst had a composition of 57 wt.% Pt and 43 wt.% carbon (Johnson Matthey) with a Pt loading of about 2 mg cm^{-2} . The anode and cathode electrodes were hot-pressed on both sides of a Nafion N-115 membrane.

2.2 Electrochemical set-up and test cell

The experiments with partitioned GDLs were performed at different operating conditions and with a grid (column) flow field geometry. Each column has a cross section of $1 \times 1 \text{ mm}^2$ and a height of 1 mm. Under counter flow conditions, air was fed at the top and methanol at the bottom of the cell. All measurements were carried out at a temperature of $70 \text{ }^\circ\text{C}$ and ambient pressure. The anode was constantly fed by a methanol solution with a concentration

of 1 mol l^{-1} and a flow rate of 2.19 ml min^{-1} . The cathode was supplied with an air flow of 378 ml min^{-1} .

The current and temperature distribution was measured with a special measurement system, consisting of a printed circuit board (PCB) that was inserted between the aluminium end plate and the graphite flow field on the anode side and special electronics outside the cell. The PCB inside the cell assembly was equipped with a gold plated segmented contact area with 25 segments on the side towards the graphite flow field and one digital temperature sensor for each segment on the other side. The segmented contact area was connected with separate measurement and excitation wires to external electronics measuring the segment currents and controlling the potential of each segment so that all segments together form an equipotential surface in order to eliminate a smoothing of the current distribution caused by the measurement system, which would occur if only shunt resistors were used for measuring the segment currents [2].

This measurement system was also used to control the cell voltage and current by adjusting the voltage between the segmented contact area on the PCB and the cathode end plate. The whole measurement system was controlled with a central computer based sequential control program that also controlled the mass flow controllers for the air flow and the peristaltic pumps for the methanol flow.

A separate program was used to record the temperature readings from the temperature sensors on the PCB inside the cell and to display the temperature distribution.

2.3 Neutron radiography

The radiography experiments were performed at the neutron tomography instrument CONRAD/V7 at Helmholtz Centre Berlin (formerly Hahn-Meitner Institute) in Germany. The instrument is located at the end of a curved neutron guide. This way only the cold neutrons –

which provide a much higher contrast than thermal neutrons – are transmitted through the neutron guide. Thermal neutrons and gamma radiation are almost completely eliminated. The imaging set-up is based on a pinhole geometry with a small variable aperture. The main part of the detector system is a 16-bit low-noise CCD camera (Andor DW436N with 2048×2048 pixel²) [24]. The camera is focused by a lens system on a neutron sensitive scintillator screen (Gadox) which was mounted close to the fuel cells to ensure high spatial resolutions down to 60 μm .

3. Results

3.1 Influence of anode gas diffusion layer wettability

First of all, MEAs with vertically split anode carbon cloth were prepared and characterized. Fig. 2 shows normalised radiographs (left hand) and the corresponding current distributions (right hand) for three different average current densities and constant flow rates. All the neutron radiographs and current distributions shown in this figure were recorded under steady state conditions, i.e. after about 1 hour. At the lowest average current density of 50 mAcm^{-2} and highest methanol and air stoichiometry of 24 (see Fig. 2a), only clusters of CO_2 bubbles appear in the anode flow field (see light spots). However, no flooding of cathode channels is observed under these conditions. The distribution of CO_2 bubbles across the anode is quite homogeneous: there is no visible difference between the left, untreated part (see blue frame) and the right, hydrophobised part (see red frame). The same is true for the current distribution, which appears to be more or less symmetrical. Thus, similar values of power generation are achieved for the left side (51 %) and the right side (49 %).

If the current density is increased to 150 mA/cm^2 (see Fig. 2b), water droplets appear in the bottom part of the cathode channels (see dark spots), but there is virtually no difference between the untreated and the hydrophobised side. Again, similar currents and power

densities are obtained for both parts of the MEA. The formation of water droplets may be explained by an increasing uptake of water vapour by the air stream from the top to the bottom of the cell. It should be considered that compared with the previous experiment, water production is three times as high but air (and methanol) flow is the same, corresponding to a reduced oxygen stoichiometry of 8. Below the upper boundary of the water droplets, oversaturation of air does not allow removing water solely as vapour and water droplets are generated in the cathode flow field channels. The removal of water droplets is governed by gravitation (droplet size), capillary forces (GDL wettability properties and pore size distribution) and the interaction of water droplets with the wall of the cathode flow field channels (channel wettability properties and geometry).

At the highest current density of 300 mA/cm^2 and the lowest air stoichiometry of 4, there is even more water in the cathode channels, preferentially in the middle part of the cell (see Fig. 2c). A tentative explanation for the latter observation is the increasing size of water droplets and their faster removal because of gravity, when they flow down and merge. Still, there is no significant difference concerning the liquid and current distribution between the untreated and hydrophobised part of the MEA. From the results of a vertically split anode GDL, it can be concluded that the wettability of anode carbon cloth only has a minor influence on the fluid transport in the DMFC anode. Therefore, MEAs with vertically split anode carbon cloth have the same performance (110 mW/cm^2 , 300 mA/cm^2) as undivided MEAs with hydrophobised anode carbon cloth.

3.2 Influence of cathode gas diffusion layer wettability

The same experiments were performed by vertically splitting the cathode carbon cloth. Again, the neutron radiographs and the corresponding current distributions are shown for three different average current densities (see Fig. 3). As above, only the data obtained under

steady state conditions are shown. At the lowest current density of 50 mA/cm^2 , only the evolution of CO_2 bubbles, but no formation of water droplets in the cathode gas channels is observable (see neutron radiograph in Fig. 3a). Nevertheless, there is a dominant power generation of about 60 % in the right, hydrophobised part of the cell (see current distribution in Fig. 3a). Hence, there is no correlation between the fluid distribution shown in the neutron radiograph and the current distribution under these conditions. This result indicates that it is not only the fluid distribution in the flow field channels that has to be considered, but also the media distribution in the underlying porous gas diffusion electrodes, which cannot be resolved in these experiments and which is also supposed to have a large influence on current distribution. Most probably, a partial flooding of the untreated carbon cloth in the left side of the MEA and subsequent blocking of the oxygen transport is responsible for the low performance of this part.

If the average current density is increased to 150 mA/cm^2 , water droplets appear preferentially in the left, untreated part of the cathode channels. Again, the left part of the cell contributes to 40 % of the overall power generation only. The time-dependent current density, power density and cell voltage during the experiment are presented in Fig. 4. Concerning current and power density, the total values as well as the data of untreated (left) part and hydrophobised (right) part are shown. As the total current is constant during the experiment, inverse curves of the currents in the untreated and the hydrophobised part of the cell are indicated in Fig. 4. Additionally, neutron radiographs are shown for different, time-dependent states of media distribution in the flow field channels. They can be compared with a neutron radiograph taken at steady state conditions in Fig. 3b.

Immediately after switching on the current, only very few, small water droplets are visible in the neutron radiograph (see Fig. 4a, $t = 0 \text{ s}$). In the following period up to about 500 s, the cell voltage, power density and current of the hydrophobised part drops, whereas the current

of the untreated part increases. This is due to a flooding of the right, hydrophobised part of the cell during that time and demonstrated by the neutron radiograph taken after 494 s, showing water droplets generated in the bottom, right part of the cathode flow field channels. After 500 s of operation, most of the water droplets disappear (not shown here). Simultaneously, U_{cell} , p , p_{right} and j_{right} increase and j_{left} decreases. The enhanced performance can easily be explained by an improved oxygen supply of the right, hydrophobised part of the cell. However, it should be emphasised that the current in the hydrophobised part of the cell is always higher than that in the untreated part, independent on visible flooding effects in the flow field channels. This result again suggests that water management of GDLs can be even more important than the liquid distribution in the flow field channels. It further suggests future experiments to be performed not only in the through plane mode, but also in the cross sectional viewing direction to visualize the liquid distribution within the GDLs. This means neutron radiography as well as synchrotron X-ray investigations.

As the experiment goes on, more and more water droplets appear in the left, untreated part of the cell (see neutron radiograph Fig. 4c). After about 1300 s, steady state conditions are achieved with some agglomeration of water droplets in the left part of the cell and almost constant cell performance. Thus, the neutron radiographs Fig. 4d (1356 s) and Fig. 3b (end of experiment) are quite similar.

The effects of water accumulation in the left part of the cathode flow field channels and the lower power generation in this part of the cell are even more pronounced at the highest average current density of 300 mA/cm^2 , shown in Fig. 3c. Water droplets appear in the cathode channels over the entire left side of the cell, causing an additional power loss: the untreated part of the cell contributes to 38 % of the total power generation only. Fig. 5 shows the time-dependent performance data for the average current density of 300 mA/cm^2 . Qualitatively, the same behaviour is obtained as compared to the results achieved at an

average current density of 150 mA/cm^2 (see Fig. 4). However, the flooding of the right, hydrophobised part of the cathode flow field (see neutron radiograph Fig. 5b) and the sudden removal of the water droplets is three times faster and the change of performance during these processes is more pronounced. After about 270 s (see neutron radiograph Fig. 5c), the amount of water in the cathode flow field channels of the left and the right part of the cell are approximately the same. It takes about 460 s, until steady state conditions are achieved and the water droplets predominantly appear in the left, untreated part of the cell (see neutron radiograph Fig. 5c).

No conclusive explanation for the observed ‘shift’ of water droplets in the cathode channels from the hydrophobised to the untreated part of the cell can be offered here. However, the three times faster process when doubling the current density suggests a mechanism, where the untreated part of the GDL behaves like a sponge, taking up water in the beginning of the experiment after switching on the current. Therefore, water removal preferentially takes place in the cathode flow field channels of the hydrophobised part of the cell during this period. When the water uptake capacity of the untreated GDL is exceeded, water droplets are released to the cathode flow field channels in this part of the cell. The higher the current density, the more water is produced in the cathode gas diffusion electrode and the faster is the process of taking up water in the untreated part of the cathode GDL. Experiments with cross sectional viewing direction and higher resolution, i.e. synchrotron X-ray investigations, are necessary to clarify the mechanism behind the observed effect.

The MEA with divided cathode carbon cloth has a performance of less than 40 mW/cm^2 (300 mA/cm^2) under steady state conditions, which is only little more than one third of the performance of undivided, standard MEAs under these conditions. This result can be explained by the restricted oxygen transport in the left, untreated part of the cell due to water accumulation in the cathode GDL and flow field channels, causing a high cathode

overpotential and a cell voltage drop. It means that the actual, low performance of the untreated part dominates the total power density of the cell.

4. Conclusions

The combination of high resolution neutron radiography and simultaneous measurement of the local current distribution provides valuable information about the influence of GDL wettability on the performance of a DMFC. It turns out that the hydrophobicity of the anode carbon cloth has practically no influence on the fluid transport in the DMFC anode and thus the performance of the MEA. In contrast, hydrophobisation of the cathode carbon cloth seems to be important, as it enables a fast removal of water droplets, facilitates the oxygen transport in the cathode GDL and cathode flow field channels and thus increases the performance. This effect is even more pronounced at high current densities. Under the abovementioned operating conditions, the fluid distribution in the porous layers of the gas diffusion electrodes appears to be crucial for the local cell performance. The water distribution in cathode GDLs cannot be resolved by neutron radiography when operating in through plane mode. In order to visualize local flooding processes in cathode GDLs, it is suggested to perform future experiments with neutron radiography and/or synchrotron X-ray investigations in the cross sectional viewing direction.

Acknowledgements

We gratefully acknowledge the financial support of this work by the German Federal Ministry of Education and Research (BMBF) under Grant No. 03SF0324.

References

- [1] C. Hartnig, L. Jörisen, W. Lehnert, J. Scholta, Direct methanol fuel cells (DMFC), *Materials for Fuel Cells*, Ed. M. Gasik, Woodhead Publishing Limited (2008) 185–208
- [2] D. U. Sauer, T. Sanders, B. Fricke, T. Baumhöfer, K. Wippermann, A. A. Kulikovskiy, H. Schmitz, J. Mergel, *Journal of Power Sources* 176 (2008) 477–483
- [3] T. Sanders, T. Baumhöfer, D. U. Sauer, A. Schröder and K. Wippermann, *ECS Transactions* 25 (2009) 1719–1728
- [4] P. Argyropoulos, K. Scott, W. M. Taama, *Electrochimica Acta* 44 (1999) 3575–3584
- [5] H. Yang, T. S. Zhao, Q. Ye, *Journal of Power Sources* 139 (2005) 79–90
- [6] C. W. Wong, T. S. Zhao, Q. Ye, J. G. Liu, *Journal of The Electrochemical Society* 152 (2005) A1600–A1605
- [7] Q. Liao, X. Zhu, X. Zheng, Y. Ding, *Journal of Power Sources* 171 (2007) 644–651
- [8] J. Inukai, K. Miyatake, Y. Ishigami, M. Watanabe, T. Hyakutake, H. Nishide, Y. Nagumo, M. Watanabe, A. Tanaka, *Chemical Communications*, (2008) 1750–1752
- [9] X. Liu, H. Guo, C. Ma, *Journal of Power Sources* 156 (2006) 267–280
- [10] X. Liu, H. Guo, F. Ye, C. Ma, *Electrochimica Acta* 52 (2007) 3607–3614
- [11] D. Spornjak, S. G. Advani, A. K. Prasad, *Journal of The Electrochemical Society*, 156 (2009) B109–B117
- [12] I. Manke, C. Hartnig, M. Grünerbel, W. Lehnert, N. Kardjilov, A. Haibel, A. Hilger, J. Banhart, H. Riesemeier, *Applied Physics Letters* 90, 174105 (2007)
- [13] C. Hartnig, I. Manke, R. Kuhn, N. Kardjilov, J. Banhart, W. Lehnert, *Applied Physics Letters* 92, 134106 (2008)

- [14] C. Hartnig, I. Manke, J. Schloesser, P. Krüger, R. Kuhn, H. Rieseheimer, K. Wippermann and J. Banhart, *Electrochemistry Communications* 11 (2009) 1559–1562
- [15] C. Hartnig, I. Manke, R. Kuhn, S. Kleinau, J. Goebbels, J. Banhart, *Journal of Power Sources* 188 (2009) 468–474
- [16] D. Kramer, E. Lehmann, G. Frei, P. Vontobel, A. Wokaun, G. G. Scherer, *Nuclear Instruments and Methods in Physics Research A* 542 (2005) 52–60
- [17] I. Manke, C. Hartnig, M. Grünerbel, J. Kaczerowski, W. Lehnert, N. Kardjilov, A. Hilger, J. Banhart, W. Treimer, M. Strobl, *Applied Physics Letters* 90, 184101 (2007)
- [18] C. Hartnig, I. Manke, N. Kardjilov, A. Hilger, M. Grünerbel, J. Kaczerowski, J. Banhart, W. Lehnert, *Journal of Power Sources* 176 (2008) 452–459
- [19] I. Manke, C. Hartnig, N. Kardjilov, M. Messerschmidt, A. Hilger, M. Strobl, W. Lehnert, J. Banhart, *Applied Physics Letters* 92, 244101 (2008)
- [20] R. J. Bellows, M. Y. Lin, M. Arif, A. K. Thompson, D. Jacobson, *Journal of The Electrochemical Society* 146 (1999) 1099–1103
- [21] M. A. Hickner, N. P. Siegel, K. S. Chen, D. S. Hussey, D. L. Jacobson, M. Arif, *Journal of The Electrochemical Society*, 155 (2008) B427–B434
- [22] P. Boillat, D. Kramer, B. C. Seyfang, G. Frei, E. Lehmann, G. G. Scherer, A. Wokaun, Y. Ichikawa, Y. Tasaki, K. Shinohara, *Electrochemistry Communications* 10 (2008) 546–550
- [23] A. Schröder, K. Wippermann, J. Mergel, W. Lehnert, D. Stolten, T. Sanders, T. Baumhöfer, D. U. Sauer, I. Manke, N. Kardjilov, A. Hilger, J. Schloesser, J. Banhart and C. Hartnig, *Electrochemistry Communications* 11 (2009) 1606–1609
- [24] N. Kardjilov, A. Hilger, I. Manke, M. Strobl, W. Treimer, J. Banhart, *Nuclear Instruments and Methods in Physics Research A* 542 (2005) 16–21

Figure captions:

Fig. 1: Scheme of GDL partitioning by vertically splitting the carbon cloth into an untreated and a hydrophobised part. The neutron radiographs always represent the view from the cathode side. The splitting of anode and cathode was done in such a way, that the untreated carbon cloth (CC) always appears on the left hand side, and the hydrophobised carbon cloth is indicated in the right hand side of the neutron radiographs.

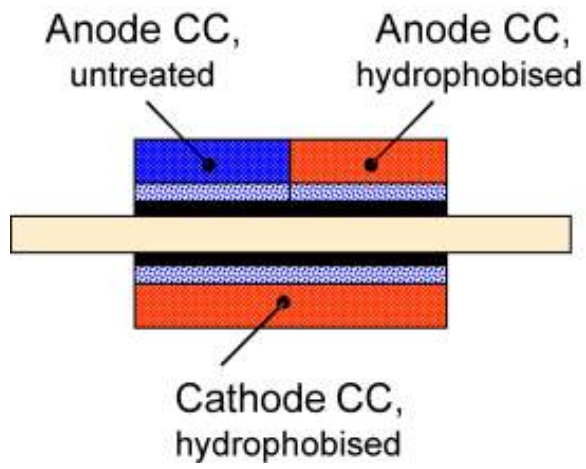
Fig. 2: Normalised radiographs (left hand) and the corresponding current distributions (right hand) of a MEA with a vertically split anode carbon cloth at current densities of 50 (a), 150 (b) and 300 mA/cm² (c). Constant flow rates of 1 molar methanol solution (2.19 ml/min) and air (378 ml/min), corresponding to methanol and oxygen stoichiometry factors of 24 (a), 8 (b) and 4 (c). All the neutron radiographs and current distributions were recorded under steady state conditions.

Fig. 3: Normalised radiographs (left hand) and the corresponding current distributions (right hand) of a MEA with a vertically split cathode carbon cloth, same operating conditions as described in the caption of Fig. 2.

Fig. 4: Time dependence of current density, power density and cell voltage during the experiment performed at a current density of 150 mA/cm² with the MEA containing a vertically split cathode carbon cloth (see Fig. 3b). In case of current and power density, total values as well as data of untreated (left) part and hydrophobised (right) part are presented. Additionally, neutron radiographs indicating characteristic states of media distribution in the flow field channels are shown.

Fig. 5: Time dependence of current density, power density and cell voltage during the experiment performed at a current density of 300 mA/cm^2 (compare Fig. 3c), same MEA and operating conditions as described in Fig. 4.

a Partitioning of Anode GDL



b Partitioning of Cathode GDL

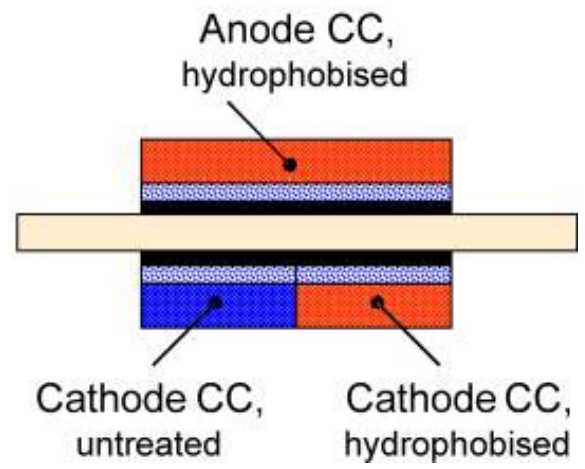


Fig. 1

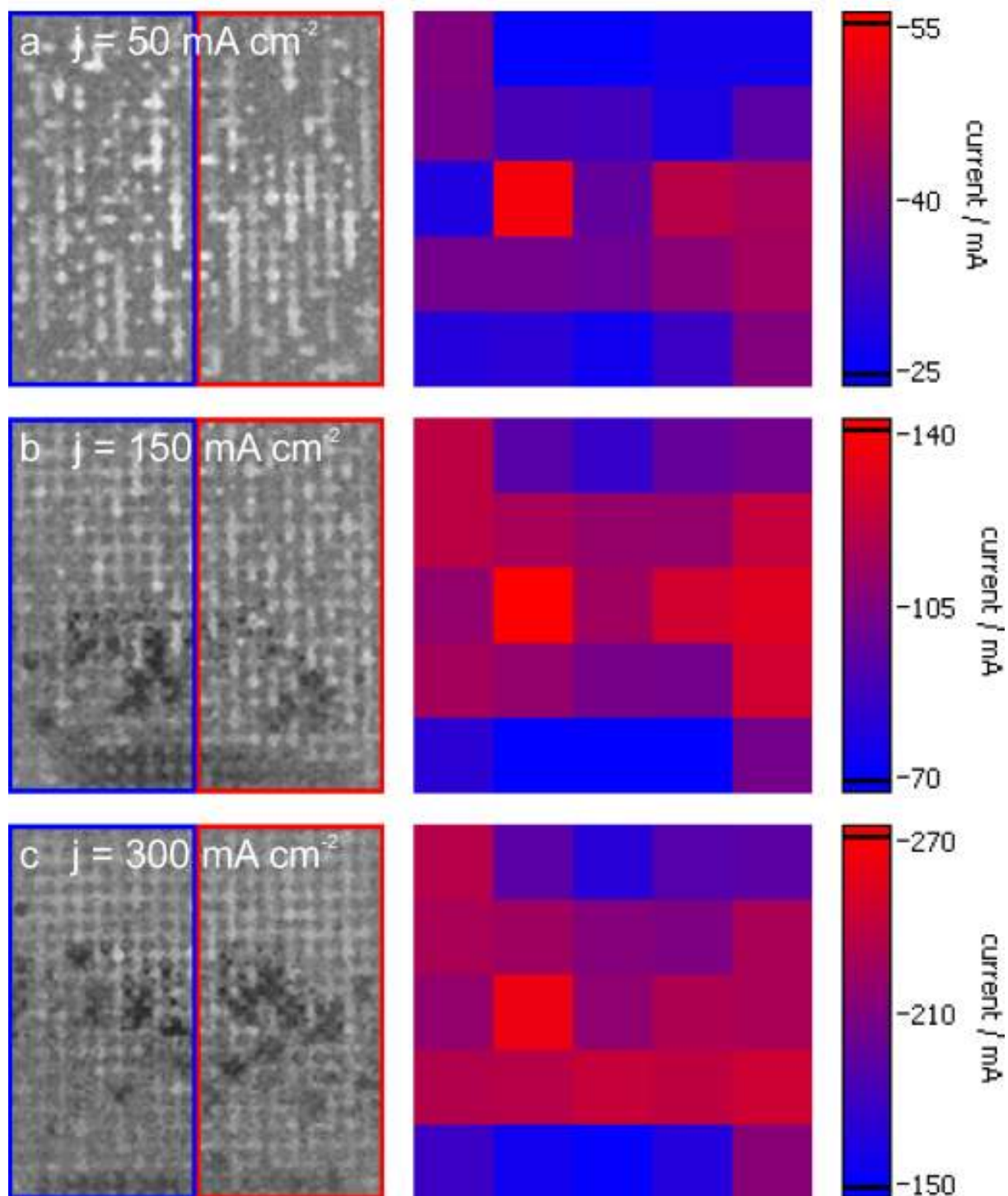


Fig. 2

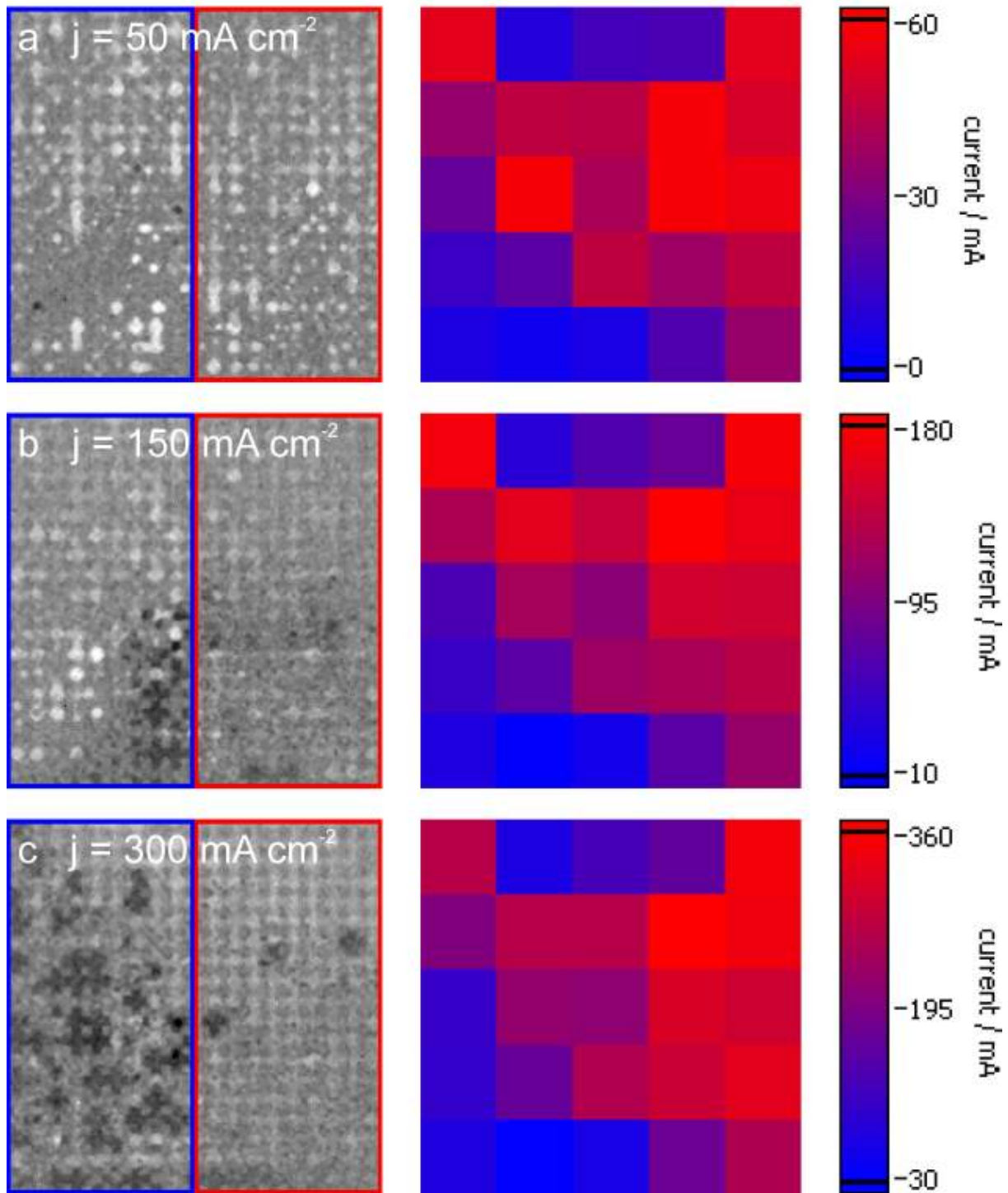


Fig. 3

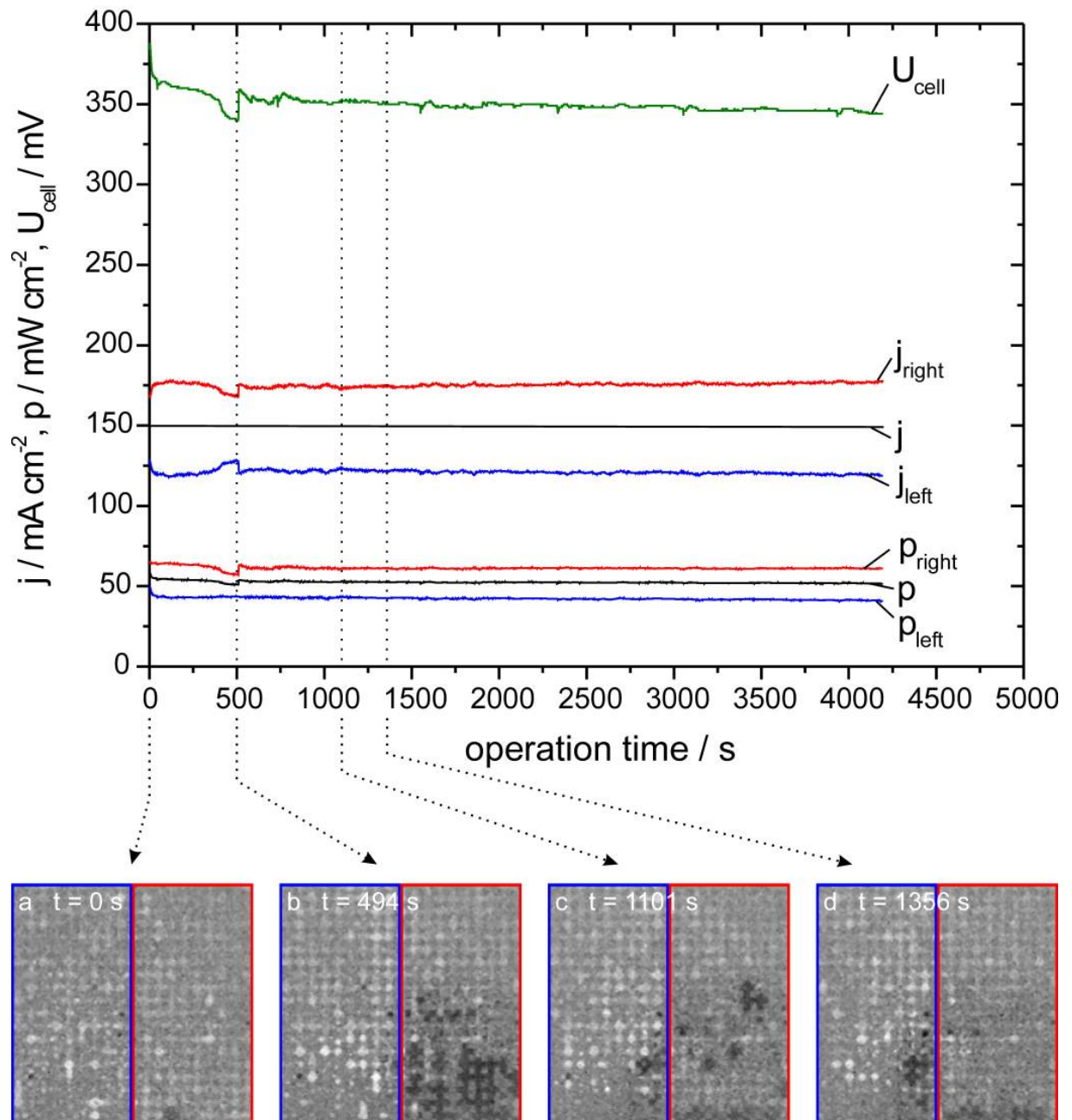


Fig. 4

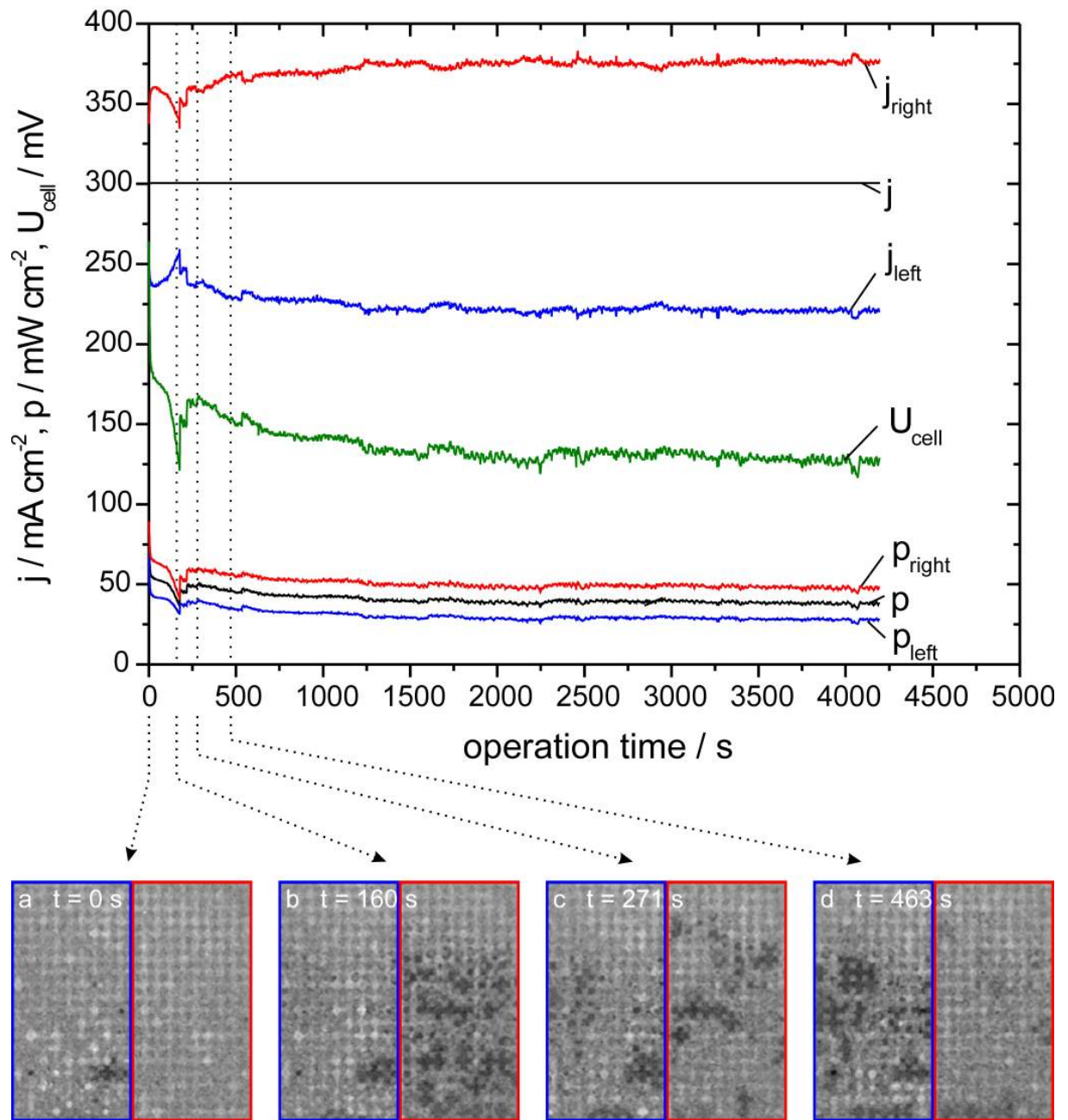


Fig. 5